ISSN 1063-7761, Journal of Experimental and Theoretical Physics, 2014, Vol. 118, No. 1, pp. 27–33. © Pleiades Publishing, Inc., 2014.
Original Russian Text © A.P. Anyutin, I.P. Korshunov, A.D. Shatrov, 2014, published in Zhurnal Eksperimental'noi i Teoreticheskoi Fiziki, 2014, Vol. 145, No. 1, pp. 35–42.

ATOMS, MOLECULES, OPTICS

The Field of a Point Source near Planar and Cylindrical Boundaries of a Metamaterial

A. P. Anyutin[a,*], I. P. Korshunov[b,], and A. D. Shatrov[b]**

[a]*Russian New University, ul. Radio 12, Moscow, 105005 Russia*
[b]*Kotel'nikov Institute of Radio Engineering and Electronics, Fryazino Branch, Russian Academy of Sciences, pl. Vvedenskogo 1, Fryazino, Moscow oblast, 141190 Russia*
**e-mail: anioutine@mail.ru*
***e-mail: korip@ms.ire.rssi.ru*

Received June 7, 2013

Abstract—The properties of the two-dimensional electromagnetic fields excited by a filamentary source located near planar and cylindrical boundaries of bodies made of metamaterials with their permittivity and permeability close to minus one are considered. The subwavelength field localization effects, the phenomena associated with the resonances of surface waves, and the nonresonant field enhancement effects are investigated.

DOI: 10.1134/S1063776114010014

1. INTRODUCTION

The electromagnetic field near a planar boundary separating media with material parameters $\varepsilon = \mu = 1$ and $\varepsilon = \mu = -1$ has unusual properties. For example, the problem of the excitation of a half-space filled with a metamaterial with parameters $\varepsilon = \mu = -1$ by a point source has no solution, and surface waves with a continuous spectrum of propagation constants exist at the interface [1]. When bodies made of metamaterials are excited by a point source located near their boundaries, surface waves whose fields cannot be described by the methods of geometrical optics emerge.

Let us discuss in more detail the properties of the wave fields near planar and curved boundaries in the two-dimensional problems of cylindrical-wave diffraction by bodies made of metamaterials whose permittivity and permeability are close or equal to minus one.

To be specific, we will consider the case of TM-polarization where the components $H_z(x, y)$, $E_x(x, y)$, and $E_y(x, y)$ are present in the electromagnetic field. The diffraction problem is reduced in this case to finding the scalar function $U(x, y) = H_z(x, y)$ that should satisfy the Helmholtz equations outside and inside the body, the corresponding boundary conditions on its surface, and the radiation conditions at infinity. The incident field $U^0(r, \varphi)$ is specified in the form

$$U^0(r, \varphi) = H_0^{(2)}[k\sqrt{r^2 + r_0^2 - 2rr_0\cos(\varphi - \varphi_0)}], \quad (1)$$

where $H_0^{(2)}$ is the Hankel function, k is the wave number in a free space, (r, φ) and (r_0, φ_0) are the polar coordinates of the observation points and the source, respectively. The time dependence of the fields is described by the factor $\exp(i\omega t)$.

2. DIFFRACTION BY A HALF-SPACE

The problem of the excitation of a half-space filled with a metamaterial (see Fig. 1) was studied analytically in [1]. In this paper, the problem was shown to have no solution at $\varepsilon = \mu = -1$. Under the assumption that ε and μ are real quantities and approach minus one along the curve $\varepsilon\mu = 1$ (for example, $\varepsilon = -1 + \delta$,

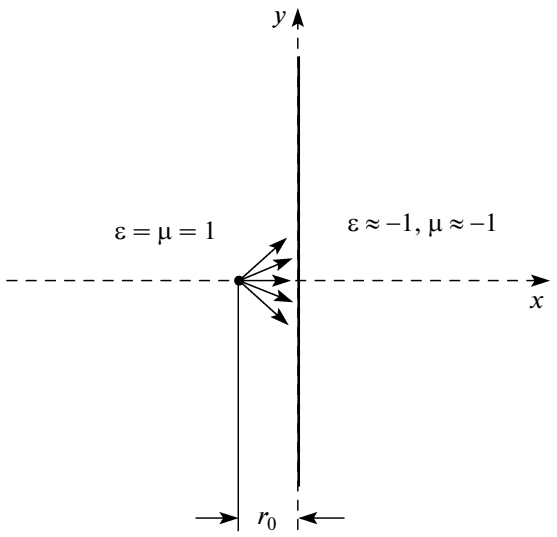

Fig. 1. Half-space filled with a metamaterial.

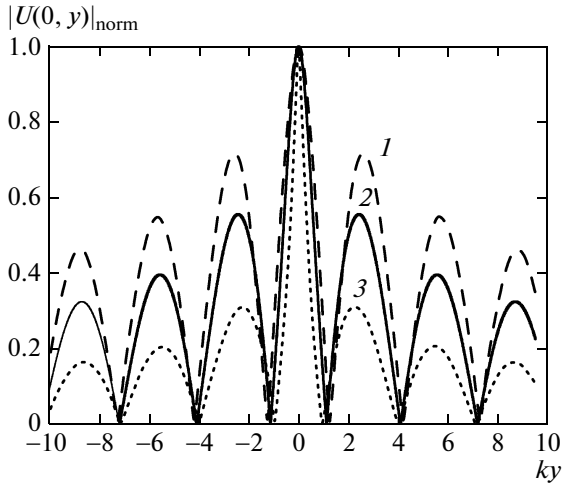

Fig. 2. Normalized distribution of the field magnitude on the $x = 0$ plane when $\varepsilon \longrightarrow -1$, $\mu \longrightarrow -1$, $r_0 = 1.0$ (*1*), 0.5 (*2*), and 0.1 (*3*).

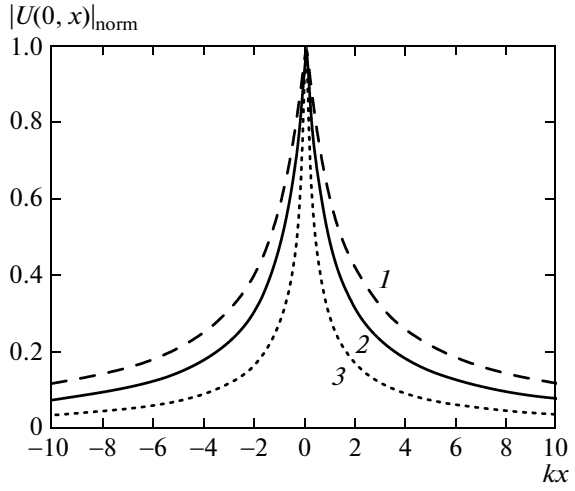

Fig. 3 Normalized distribution of the field magnitude along the line $y = 0$ when $\varepsilon \longrightarrow -1$, $\mu \longrightarrow -1$, $r_0 = 1.0$ (*1*), 0.5 (*2*), and 0.1 (*3*).

$\mu = -1 - \delta$, $|\delta| \longrightarrow 0$), it was established that the field increases indefinitely according to the law

$$U(x, y) = \frac{2i}{\varepsilon + 1} V(x, y) = \frac{2i}{\delta} V(x, y), \qquad (2)$$

where the function $V(x, y)$ is defined by the integral

$$V(x, y) = \frac{2}{\pi} \int_k^\infty \frac{1}{\sqrt{h^2 - k^2}} \times \exp[-\sqrt{h^2 - k^2}(r_0 + |x|)] \cos(hy) dh, \qquad (3)$$

where h is the transverse propagation constant.

The three-dimensional problem of the excitation of a half-space made of a metamaterial by an electric dipole parallel to the interface between the media was studied numerically in [2, 3]. The metamaterial was assumed to have small heat losses: $\varepsilon = -1 - i\delta$ and $\mu = -1 - i\delta$. The field was shown to increase when $\delta \longrightarrow 0$ according to the law $1/\delta$, which is consistent with Eq. (2) (in these calculations, the losses reached very small values, $\delta \sim 10^{-10}$).

Integral (3) can be written in an equivalent form that is more convenient for numerical calculations:

$$V(x, y) = -N_0[k\sqrt{(r_0 + |x|)^2 + y^2}] + \frac{2}{\pi} \int_0^{\pi/2} \sin[k(r_0 + |x|)\cos t] \cos(ky \sin t) dt, \qquad (4)$$

where N_0 is the Neumann function.

Figure 2 presents normalized distributions of the fields along the interface $x = 0$ for various values of the parameter kr_0 that characterizes the source's distance from the interface $x = 0$. The field has a multilobe interference pattern and is concentrated near $y = 0$. Both the width of the main lobe and the level of the side lobes decrease with decreasing parameter kr_0.

It follows from Eq. (4) that the coordinate dependence of the field at $y = 0$ is described by the expression

$$V(x, 0) = -N_0(kr_0 + |kx|) + \mathbf{H}_0(kr_0 + |kx|), \qquad (5)$$

where $\mathbf{H}_0$ is the Struve function [4]. Figure 3 shows normalized graphs of functions (5) for various values of the parameter kr_0. It can be seen from the figure that the fields decrease monotonically with increasing distance from the interface between the media and have a form typical of surface waves.

It follows from Eq. (2) and Figs. 2 and 3 that there is subwavelength field localization at the point with $x = 0$ and $y = 0$ when $\varepsilon \longrightarrow -1$ and $\mu \longrightarrow -1$, i.e., the field is concentrated in a region whose size is considerably smaller than the wavelength $\lambda = 2\pi/k$.

Recall that, according to (2), the field increases indefinitely when $\varepsilon \longrightarrow -1$, and, consequently, its value at the point with $x = 0$ and $y = 0$ can exceed considerably the magnitude of the exciting field at this point $H_0^{(2)}(kr_0)$.

3. DIFFRACTION BY A CIRCULAR CYLINDER

Consider the problem of diffraction by a circular cylinder of radius a with parameters $\varepsilon < 0$ and $\mu < 0$ (see Fig. 4).

This problem admits an analytical solution by the variable separation method (Rayleigh series [5]). In

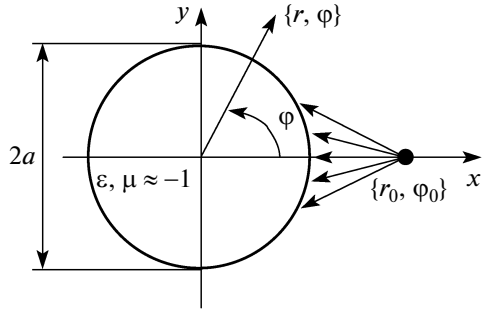

Fig. 4. Metamaterial cylinder; the geometry of the problem.

particular, the field inside the cylinder can be written as [6]

$$U(r,\varphi) = -\frac{2i}{\pi ka} \times \sum_{m=0}^{\infty} \delta_m H_m^{(2)}(kr_0) J_m(knr)\cos(m\varphi) \times \left\{ H_m^{(2)'}(ka) J_m(kna) - \frac{n}{\varepsilon} H_m^{(2)}(ka) J_m'(kna) \right\}^{-1}, \quad r < a, \tag{6}$$

where

$$\delta_m = \begin{cases} 1, & m = 0, \\ 2, & m \geq 1, \end{cases} \tag{7}$$

$$n = \sqrt{\varepsilon\mu}, \tag{8}$$

J_m is the Bessel function; the prime denotes differentiation with respect to the argument.

The field outside the cylinder ($r \geq a$) consists of two terms, the incident and scattered fields:

$$U(r,\varphi) = U^0(r,\varphi) + U^s(r,\varphi). \tag{9}$$

The scattered field U^s in the far field zone ($kr \longrightarrow \infty$) is

$$U^s(r,\varphi) \sim \Phi^s(\varphi)\left(\frac{2}{\pi kr}\right)^{1/2} \exp\left(-ikr + \frac{i\pi}{4}\right), \tag{10}$$

where $\Phi^s(\varphi)$ is the scattering pattern. The pattern of the incident field $U^0(r, \varphi)$ is expressed by the formula

$$\Phi^0(\varphi) = \exp(ikr_0\cos\varphi). \tag{11}$$

We will not provide the formulas that were used to calculate the field outside the cylinder and to calculate the scattered field pattern; they are contained in [6].

Note that the convergence of series (6) slows down significantly at $\varepsilon = \mu = -1$ and $ka \gg 1$. The behavior of the denominator in Eq. (6) when $m \longrightarrow \infty$ is responsible for this. At $\varepsilon = \mu = -1$, we have

$$H_m^{(2)'}(ka) J_m(kna) - \frac{n}{\varepsilon} H_m^{(2)}(ka) J_m'(kna) = H_m^{(2)'}(ka) J_m(ka) + H_m^{(2)}(ka) J_m'(ka) = \frac{d}{d(ka)}[H_m^{(2)}(ka) J_m(ka)]. \tag{12}$$

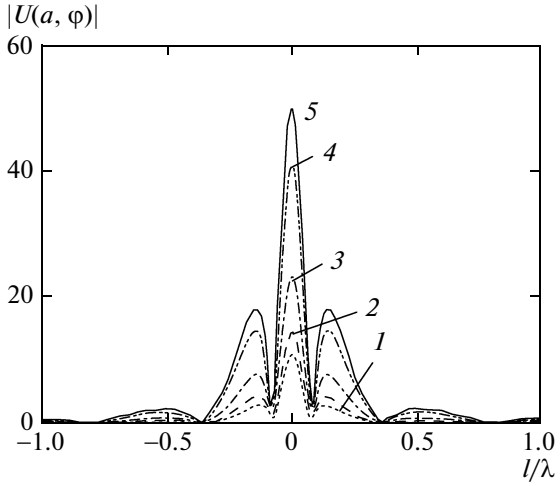

Fig. 5. Distribution of the field magnitude on the cylinder surface for $\varepsilon = \mu = -1$, $kr_0 = ka + 1.0$, $ka = 2.4$ (*1*), 4 (*2*), 8 (*3*), 16 (*4*), 20 (*5*); $l/\lambda = ka\varphi/2\pi$.

For $m \gg ka \gg 1$, the following asymptotic representations are valid [4]:

$$J_m(ka) \sim \frac{1}{\sqrt{2\pi m}}\left(\frac{eka}{2m}\right)^m, \quad H_m^{(2)}(ka) \sim i\sqrt{\frac{2}{\pi m}}\left(\frac{eka}{2m}\right)^{-m}. \tag{13}$$

Therefore,

$$H_m^{(2)}(ka) J_m(ka) \sim \frac{i}{\pi m} \tag{14}$$

and, consequently, the principal term of the denominator of asymptotic form (12) becomes zero when $m \longrightarrow \infty$, which explains why the convergence of series (6) deteriorates.

The numerical results presented below were obtained both by summing the Rayleigh series and using a modified method of discrete sources [7, 8]. The results of these calculations are in complete agreement with one another.

Figure 5 shows the distributions of the field magnitude along the cylinder surface. Curves *1*–*5* correspond to different diameters of the cylinder. The distance from the source to the cylinder surface was assumed to be fixed and equal to $k(r_0 - a) = 1$. It can be seen that the field is concentrated in the direction to the source ($\varphi = 0$) and that the spot size determined from the distance between adjacent field minima is the same for all curves and approximately equal to $\lambda/10$, i.e., the subwavelength field localization effect manifests itself.

The field concentration near the cylindrical surface is also observed along the normal to it. This can be

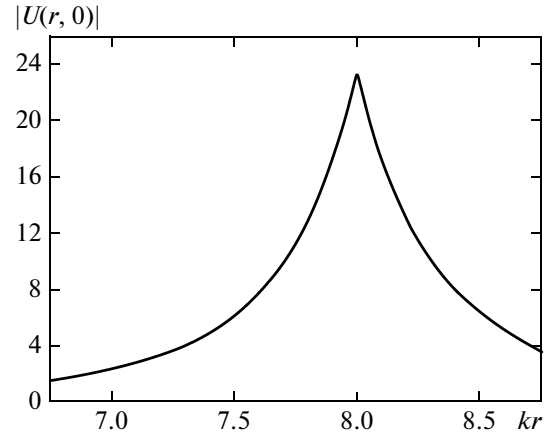

Fig. 6. Radial distribution of the field magnitude in a cylinder made of a metametarial with parameters $\varepsilon = \mu = -1$, $ka = 8$, $kr_0 = 9.0$, and $\varphi = 0$.

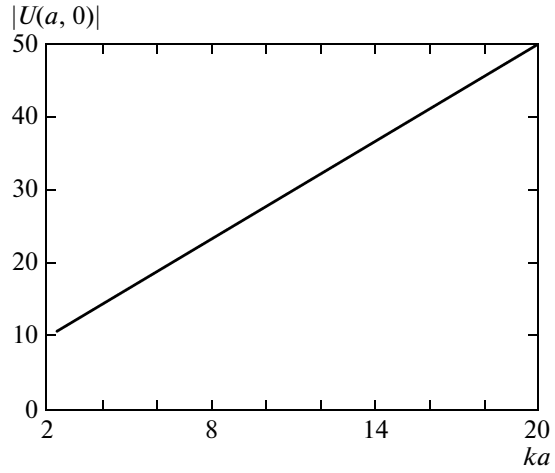

Fig. 7. Maximum field magnitude on the cylinder surface versus radius for $\varepsilon = \mu = -1$, $kr_0 = ka + 1.0$, and $\varphi = 0$.

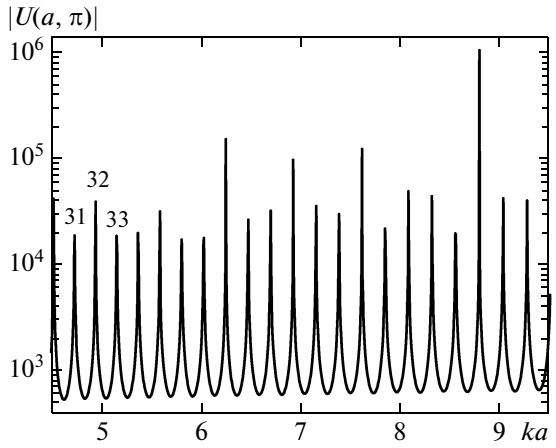

Fig. 8. AFC of a cylinder made of a metamaterial with parameters $\varepsilon = -1.001$, $\mu = -0.98$; $kr_0 = ka + 0.15$; $\varphi = \pi$.

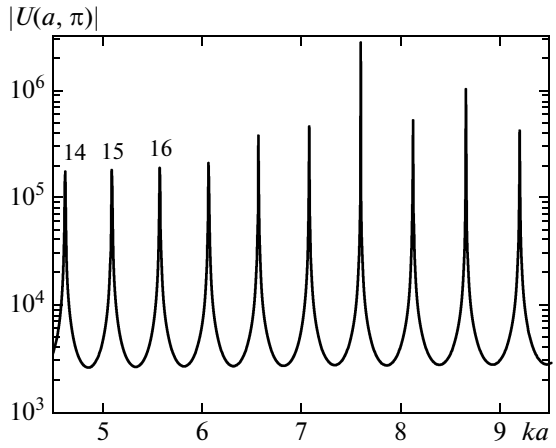

Fig. 9. AFC of a cylinder made of a metamaterial with parameters $\varepsilon = -1.01$, $\mu = -0.98$; $kr_0 = ka + 0.15$; $\varphi = \pi$.

seen from Fig. 6, where the dependence of the field on radial coordinate $|U(r, 0)|$ is plotted for $ka = 8$ and $k(r_0 - a) = 1$. At other values of ka specified in Fig. 5, the behavior of the $|U(r, 0)|$ distribution is retained; only the field amplitude at maximum changes. Qualitatively, the behavior of the field near a cylindrical boundary coincides with its behavior near a planar boundary (see Fig. 3). As in the case of a planar boundary, there is subwavelength field localization here at the point with $r = a$ and $\varphi = 0$ [9]. It follows from the calculations presented in [9] that the field decreases monotonically with increasing distance from the surface into the cylinder and no "focusing" effects following from approximate representations of geometrical optics exist. The problem of diffraction by a large-size cylinder excited by the field of a distant point source was investigated by the modified method of discrete sources in [10]. A clear physical interpretation of the results based on the method of geometrical optics is given in [10].

The field increases monotonically with increasing cylinder radius a, as can be seen from Fig. 7. Such a behavior of the field is consistent with the results of the previous section, from which it follows that the cylindrical surface passes into a planar boundary when $a \longrightarrow \infty$, and the diffraction problem has no solution in this case.

The pattern of the field distribution in space and the dependence of its amplitude on the frequency of the exciting source change radically at small deviations of ε and μ from minus one. Let us demonstrate this using the following examples.

We will describe the behavior of the field in the frequency band by the amplitude–frequency characteristic (AFC), by which we will mean the dependence of the field magnitude on the cylinder surface at the point with $r = a$ and $\varphi = \pi$ on the dimensionless parameter

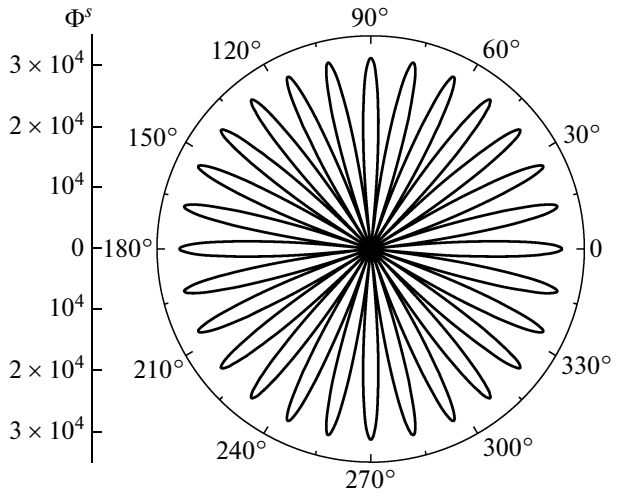

Fig. 10. Scattered field pattern $\Phi^s(\varphi)$ for a cylinder at $\varepsilon = -1.01$, $\mu = -0.98$; $ka = 4.62778205$; $kr_0 = ka + 0.15$.

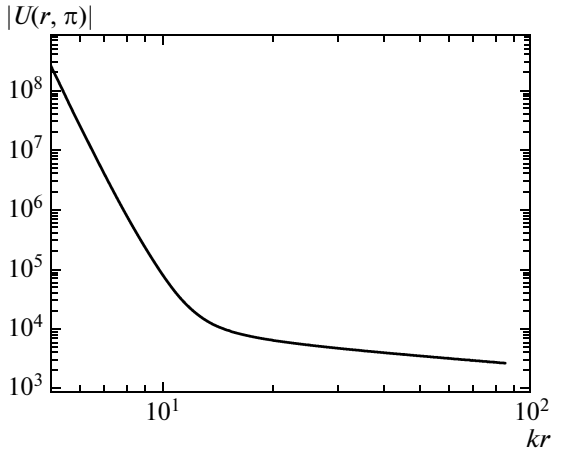

Fig. 11. Radial distribution of the magnitude of the total field outside the cylinder at $\varepsilon = -1.01$, $\mu = -0.98$; $ka = 4.62778205$; $kr_0 = ka + 0.15$.

ka. We neglect the frequency dispersion of the metamaterial.

Figures 8 and 9 show the AFCs of cylinders with parameters

$$\varepsilon = -1.001, \quad \mu = -0.98 \tag{15}$$

and

$$\varepsilon = -1.01, \quad \mu = -0.98. \tag{16}$$

The curves in Figs. 8 and 9 are the sequences of almost equidistant resonance peaks. Despite the fact that the material parameters (15) and (16) are very close, the curves in Figs. 8 and 9 differ by the number of resonances in the same frequency interval by more than a factor of 2. The field distribution along the cylinder surface and the scattering pattern at each of the resonance frequencies are described with a high accuracy by only one azimuthal harmonic $\cos(m\varphi)$. The indices m coincident with the resonance numbers in Figs. 8 and 9 (they are indicated for the three lowest resonances) also differ by a factor of 2.

It is important to note that the amplitude of the harmonic $\cos(m\varphi)$ is very large in the near field ($\sim 10^8$–10^9) and remains fairly large in the far field ($\Phi^s(\varphi)$ is $\sim 10^4$, see Fig. 10). Note that the magnitude of the incident field pattern $\Phi^0(\varphi)$ is equal to one.

Figure 11 shows the radial distribution of the magnitude of the total field along the direction $\varphi = \pi$ at the same parameters as those in Fig. 10. It can be seen that the curve contains two segments, $kr < 10$ and $kr > 20$, on which the field is described by the functions $|U| \sim (kr)^{-m}$ and $|U| \sim (kr)^{-1/2}$. These segments correspond to the near and far field zones of the diffraction field.

The effects being discussed can be explained by considering the cylinder as a ring resonator for surface waves. Indeed, an undamped surface wave with a propagation constant h that is determined from the following relation [1] can propagate along the planar boundary of a half-space filled with a medium with parameters $\varepsilon < 0$ and $\mu < 0$:

$$\frac{h^2}{k^2} = \frac{\varepsilon(\varepsilon - \mu)}{\varepsilon^2 - 1}. \tag{17}$$

The values of the material parameters at which this surface wave exist are in the third quadrant of the (ε, μ) plane and lie in regions *1* and *2* located between the two lines intersecting at point $(-1, -1)$: the vertical straight line $\varepsilon = -1$ and the hyperbola $\mu = 1/\varepsilon$ (see Fig. 12). In these domains, Eq. (17) simultaneously satisfies the conditions

$$\frac{h^2}{k^2} > 1, \quad \frac{h^2}{k^2} > \varepsilon\mu,$$

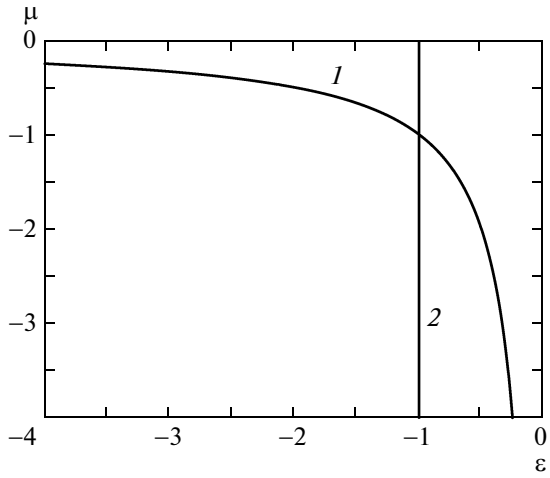

Fig. 12. Regions of existence of surface waves.

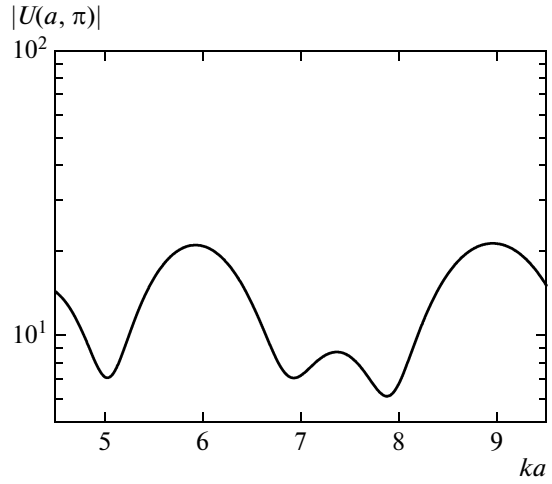

Fig. 13. AFC of a cylinder made of a metamaterial with parameters $\varepsilon = -0.98$, $\mu = -1.001$; $kr_0 = ka + 0.15$; $\varphi = \pi$.

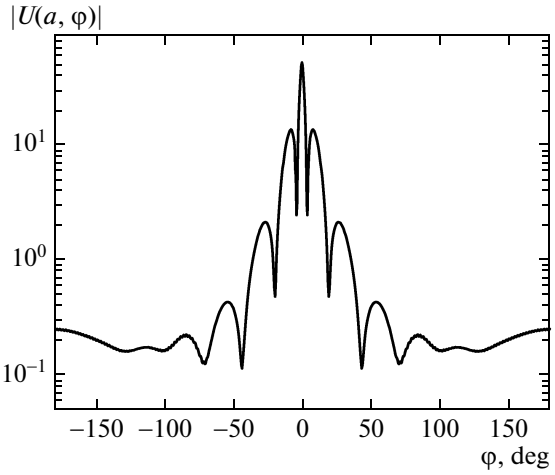

Fig. 14. Magnitude of the scattered field on the surface of a cylinder made of a metamaterial with parameters $\varepsilon = -0.98$, $\mu = -1.001$; $ka = 6$, $kr_0 = 6.15$.

i.e., the conditions for a decrease of the surface-wave field with increasing distance from the interface between the media.

At $ka \gg 1$, we can neglect the curvature of the cylinder surface and determine the resonance frequencies of the ring resonator from the relation $ha = m$, whence, given Eq. (17), the formula for the distance between adjacent resonance frequencies follows:

$$\Delta(ka) = \sqrt{\frac{\varepsilon^2 - 1}{\varepsilon(\varepsilon - \mu)}}. \qquad (18)$$

The material parameters (15) and (16) lie in the region of existence of the surface wave, and we will obtain, respectively, $\Delta(ka) \approx 0.3$ and 0.8 from Eq. (18) for these parameters. Note that the distances between adjacent resonances in Figs. 8 and 9 in the range of high frequencies are $\Delta(ka) \approx 0.25$ and 0.6. Thus, the planar boundary model allows the resonance properties of a metamaterial cylinder to be described qualitatively.

Let us show that going away from the regime of existence of surface waves changes fundamentally the spatial and frequency distributions of the field. Let us choose the following values of the material parameters that are outside regions *1* and *2* in Fig. 12:

$$\varepsilon = -0.98, \quad \mu = -1.001. \qquad (19)$$

The AFC shown in Fig. 13 corresponds to this case. We see that, in contrast to the curves in Figs. 8 and 9, it contains no high-Q resonances. In addition, the subwavelength field localization effect clearly manifests itself at these values of the parameters, as can be seen from Fig. 14 that presents the field distribution on the cylinder surface at the frequency point $ka = 6$. Thus, this effect takes place not only at $\varepsilon = \mu = -1$ but also in some region of parameters ε and μ near point $(-1, -1)$.

It also follows from Fig. 14 that the local maxima of the field $U(a, \varphi)$ on the cylinder surface exceed considerably the amplitude of the incident field $U^0(a, \varphi)$ at these points. Therefore, we can also talk about the nonresonant electromagnetic field enhancement effect on a cylindrical metamaterial boundary. Recall that the field at the boundary increases with increasing cylinder radius a (see Fig. 7). The limiting case of this effect is illustrated by the problem of diffraction by a half-space with parameters $\varepsilon = \mu = -1$, when the field enhancement factor becomes infinitely large.

Figure 15 presents the scattering pattern for a cylinder with parameters (19). The pattern contains a large number of lobes with different amplitudes and widths. Since the amplitudes of the lobes exceed one, the contribution from the incident field in the far field

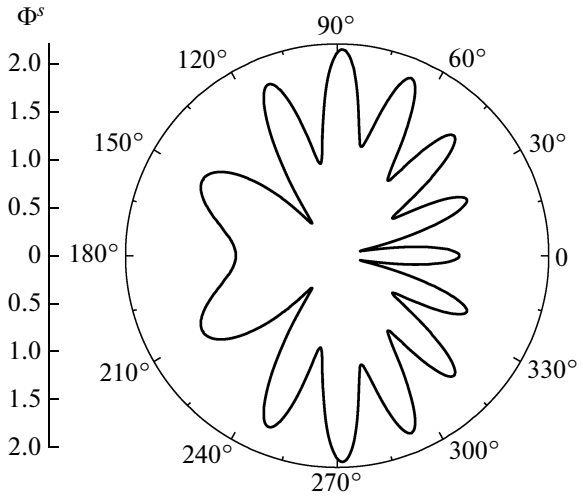

Fig. 15. Magnitude of the scattering diagram for a cylinder made of a metamaterial at $\varepsilon = -0.98$, $\mu = -1.001$; $ka = 9.5$, $kr_0 = 9.65$.

zone may be neglected, which is a confirmation of the nonresonant field enhancement effect.

4. CONCLUSIONS

We investigated the spatial structure and spectral properties of the electromagnetic fields near the boundaries of bodies made of metamaterials. The electromagnetic field emerging when a cylinder made of a metamaterial with electrodynamic parameters $\varepsilon \longrightarrow -1$ and $\mu \longrightarrow -1$ is excited by a point source was shown to depend significantly on the direction along which these parameters in the (ε, μ) plane approach the singular point $(-1, -1)$. We investigated the field properties in the frequency band. We established the regions of parameters where high-Q resonances exist. The field at the resonance frequency was shown to be concentrated near the boundary and to be described with a high accuracy by one azimuthal harmonic $\cos(m\varphi)$. We found and investigated nonresonant regimes characterized by the field concentration not only near but also along the boundary. These regimes are accompanied by subwavelength field localization, when the spot size can be $\sim\lambda/10$, and by nonresonant enhancement, when the total field at the metamaterial boundary can exceed considerably the magnitude of the incident field in a wide frequency band.

ACKNOWLEDGMENTS

This work was supported in part by the Russian Foundation for Basic Research (project no. 12-02-00062-a).

REFERENCES

1. A. D. Shatrov, J. Commun. Technol. Electron. **52** (8), 842 (2007).
2. A. B. Petrin, JETP Lett. **87** (9), 464 (2008).
3. A. B. Petrin, J. Exp. Theor. Phys. **107** (3), 364 (2008).
4. M. Abramowitz and I. A. Stegun, *Handbook of Mathematical Functions with Formulas, Graphs, and Mathematical Tables* (Dover, New York, 1972; Nauka, Moscow, 1979).
5. B. Z. Katsenelenbaum, *High-Frequency Electrodynamics* (Wiley, Weinheim, Germany, 2006).
6. A. P. Anyutin, I. P. Korshunov, and A. D. Shatrov, Tech. Phys. **84** (2014).
7. A. G. Kyurkchan, S. A. Minaev, and A. L. Soloveichik, J. Commun. Technol. Electron. **46** (6), 615 (2001).
8. A. P. Anyutin, A. G. Kyurkchan, and S. A. Minaev, J. Commun. Technol. Electron. **47** (8), 864 (2002).
9. A. P. Anyutin, I. P. Korshunov, and A. D. Shatrov, J. Commun. Technol. Electron. **58** (7), 691 (2013).
10. A. P. Anyutin, J. Commun. Technol. Electron. **56** (9), 1029 (2011).

Translated by V. Astakhov